Experimental and Theoretical Characterization of the Magnetic Properties of $CuF_2(H_2O)_2(pyz)$ (pyz = pyrazine): A Two-Dimensional Quantum Magnet Arising from Supersuperexchange Interactions through Hydrogen Bonded Paths

Jamie L. Manson,*,† Marianne M. Conner,† John A. Schlueter,‡ Amber C. McConnell,† Heather I. Southerland,† Isabelle Malfant,§ Tom Lancaster,‖ Stephen J. Blundell,‖ Michael L. Brooks,‖ Francis L. Pratt,⊥ John Singleton,# Ross D. McDonald,# Changhoon Lee,∇ and Myung-Hwan Whangbo∇

Department of Chemistry and Biochemistry, Eastern Washington University, Cheney, Washington 99004, Materials Science Division, Argonne National Laboratory, Argonne, Illinois 60439, Maître de Conférences de l'Université Paul Sabatier, Laboratoire de Chimie de Coordination - CNRS UPR 8241, 31077 Toulouse CEDEX, France, Clarendon Laboratory, Physics Department, Oxford University, Oxford OX1 3PU, U.K., ISIS Facility, Rutherford-Appleton Laboratory, Chilton, Didcot OX11 0QX, U.K., National High Magnetic Field Laboratory, Los Alamos National Laboratory, Los Alamos, New Mexico 87545, and Department of Chemistry, North Carolina State University, Raleigh, North Carolina 27695

Received June 17, 2008. Revised Manuscript Received October 21, 2008

The structural, electronic, and magnetic properties of the new linear chain coordination polymer $CuF_2(H_2O)_2(pyz)$ (pyz = pyrazine) were determined by single crystal X-ray diffraction at various temperatures, SQUID magnetometry, pulsed-field magnetization, ESR, muon-spin relaxation (μSR), and electronic structure calculations. Each Cu^{2+} ion of $CuF_2(H_2O)_2(pyz)$ is located at a distorted $CuF_2O_2N_2$ octahedron with axial elongation along the Cu−N bonds. These octahedra are tethered together by strong F···H−O hydrogen bonds to yield two-dimensional (2D) square nets in the *bc*-plane that are linked along the *a*-direction by pyrazine linkages. Measurements of the *g*-factor by ESR along with first principles density functional theory electronic structure calculations show that the magnetic orbital of the Cu^{2+} ion lies in the CuF_2O_2 plane thus forming a 2D antiferromagnetic square lattice. A broad maximum observed in $\chi(T)$ at 10 K indicates a modest spin exchange interaction through the Cu−F···H−O−Cu supersuperexchange paths, and a theoretical fit of $\chi(T)$ to a 2D square model gives $J_{2D}/k_B = -5.58(1)$ K (in the convention where *J* rather than 2*J* is used for spin exchange). At lower temperatures, $\chi(T)$ shows a sharp peak at ~2.6 K, which signals a transition to a long-range magnetic ordering as confirmed by coherent precession of implanted muons. Isothermal $M(B)$ measurements made at 0.5 K on an aligned single crystal reveal magnetic saturation, M_{sat}, at 28.8 T ($B\|a$) while a higher field of 33.1 T is required to saturate the spins when *B* is applied perpendicular to the *a*-axis thus showing clear anisotropy in these orientations. The presence of strong hydrogen bonds in $CuF_2(H_2O)_2(pyz)$ causes the chains to adopt a tilted packing arrangement, thus leading to a novel ground-state likely characterized by spin-canting within the 2D layers and a markedly increased critical temperature relative to the well-known $Cu(NO_3)_2(pyz)$ polymer chain compound.

1. Introduction

The design, synthesis, and characterization of molecular magnetic materials continues to excite much research interest around the world.[1] This interest stems largely from their mild laboratory preparations and the potential to tune or modulate their bulk magnetic properties by subtle synthetic variations. Furthermore, these materials provide convenient testing grounds for fundamental quantum many-body phenomena. An effective strategy to design novel molecular/polymeric magnets uses paramagnetic transition metal cations and a variety of organic bridging ligands such as pyrazine (pyz) with the intent of producing new structural motifs that present interesting magnetic properties.[2] Examples of such systems include complex one-dimensional (1D), two-dimensional

---

* Corresponding author. E-mail: jmanson@ewu.edu. Tel: +(509)359-2878. Fax: +(509)359-6973.
† Eastern Washington University.
‡ Argonne National Laboratory.
§ CNRS UPR 8241.
‖ Oxford University.
⊥ Rutherford-Appleton Laboratory.
Los Alamos National Laboratory.
∇ North Carolina State University.

(1) See for example: (a) *Magnetism: Molecules to Materials*; Miller, J. S., Drillon, M., Eds.; Wiley-VCH: New York, 2001−2005; Vol. 1−5. (b) Blundell, S. J.; Pratt, F. L. *J. Phys.: Condens. Matter* **2004**, *16*, R771. (c) Kahn, O. *Molecular Magnetism*; Wiley-VCH: New York, 1993. (d) Caneschi, A.; Gatteschi, D.; Sessoli, R.; Rey, P. *Acc. Chem. Res.* **1989**, *22*, 392. (e) Miller, J. S.; Epstein, A. J. *Angew. Chem., Int. Ed. Engl.* **1994**, *33*, 385. (f) Miller, J. S.; Manson, J. L. *Acc. Chem. Res.* **2001**, *34*, 563.

(2) For example, (a) Manson, J. L.; Conner, M. M.; Schlueter, J. A.; Lancaster, T.; Blundell, S. J.; Brooks, M. L.; Pratt, F. L.; Papageorgiou, T.; Bianchi, A.; Wosnitza, J.; Whangbo, M.-H. *Chem. Commun.* **2006**, 4894. (b) Manson, J. L.; Lecher, J. G.; Gu, J.; Geiser, U.; Schlueter, J. A.; Henning, R.; Wang, X.; Schultz, A. J.; Koo, H.-J.; Whangbo, M.-H. *Dalton Trans.* **2003**, 2905.

10.1021/cm8016566 CCC: $40.75

(2D), and three-dimensional (3D) arrays of Cu^{2+} ($S = 1/2$) ions that are linked via bridging diazine ligands along different directions. The judicious selection of appropriate metal/ligand/anion/solvent combinations can lead to a rich variety of structural arrangements and magnetic behaviors. For instance, $Cu(NO_3)_2(pyz)$ that forms 1D linear chains in which CuN_2O_4 octahedra are linked via intervening pyz ligands[3] undergoes a transition to long-range magnetic order below $T_N = 0.107(1)$ K.[4] Use of the formate ion (HCO_2^-) instead of the nitrate ion affords $Cu(HCO_2)_2(pyz)$ with the same type of linear Cu−pyz−Cu chains. In this case, the formate O-atoms form additional bridges between Cu^{2+} sites, thus producing a complex 3D framework that magnetically orders at a much higher temperature of 1.95 K.[2b,5] Alternatively, the pyz ligand can be exchanged with pyrimidine (pym) to yield $Cu(HCO_2)_2(pym)$ that is nearly isostructural to $Cu(HCO_2)_2(pyz)$.[6] The essential difference between the two formate compounds is the Cu−L−Cu bridge type in which L = pyz facilitates an exchange coupling constant of −3.9 K while L = pym affords $J/k_B = -26.9$ K.[2b,6]

In addition to the complex structures described above, we and others[7] have utilized halides as simple monatomic building blocks. For instance, appropriate combinations of Cl^- or Br^- anions and Cu^{2+} cations lead to rectangular lattice antiferromagnets of the type $CuX_2(pyz)$ that are comprised of intersecting bibridged $Cu-X_2-Cu$ and Cu−pyz−Cu chains.[8] Other motifs such as dimers and ladders have also been reported.[9] By comparison, the fluoride ion has been explored to a lesser extent. In a recent study, we utilized HF_2^- as a ligand to prepare 3D polymeric $[Cu(HF_2)(pyz)_2]BF_4$ in which 2D $[Cu(pyz)_2]^{2+}$ sheets are linked with HF_2^- anions.[2a] Herein, we report on the use of F^- and its potential to form strong hydrogen bonds with coordinated H_2O ligands. This idea led to the creation of yet another novel compound with the chemical formula $CuF_2(H_2O)_2(pyz)$. Its structure is reminiscent of $Cu(NO_3)_2(pyz)$, but the presence of additional hydrogen bonding interactions in $CuF_2(H_2O)_2(pyz)$ leads to long-range spin-canted antiferromagnetic ordering below ~2.6 K compared to the T_N-value of 0.107(1) K observed in the *bis*-nitrate compound.[4] In the case of $CuF_2(H_2O)_2(pyz)$, the supersuperexchange[10] interactions between the magnetic Cu^{2+} ions are facilitated by the strong F···H−O hydrogen bonds. $CuF_2(H_2O)_2$ possesses a similar Cu−F···H−O−Cu hydrogen bonding scheme, but additional Cu−F−Cu interactions also contribute to its observed magnetic behavior ($T_N = 10.92$ K) in contrast to $CuF_2(H_2O)_2(pyz)$.[11] We note that the analogous $CuCl_2(H_2O)_2(pyz)$ or $CuBr_2(H_2O)_2(pyz)$ compounds have not been reported.

2. Experimental Section

Synthesis. In a Teflon beaker, NH_4F (0.2222 g, 6 mmol) and pyrazine (0.2403 g, 3 mmol) were dissolved together in 3 mL of water. A filtered 5-mL aqueous solution containing 0.6977 g (3 mmol) of $Cu(NO_3)_2 \cdot yH_2O$ was then added yielding a pale blue solution. Pale blue blocks begin to appear within 30 min after mixing the reagents. After ~6 h, the solid was collected via vacuum filtration and air-dried for a short time. Crystals are routinely obtained in high yields (>75%). As a precaution against possible solvent loss, crystals were stored in a freezer after harvest. *CAUTION: ammonium fluoride is highly corrosive and should be handled with care!* Anal. Calcd (%) for $C_4H_8N_2O_2F_2Cu$: C, 22.07; H, 3.70; N, 12.87. Found: C, 22.15; H, 3.67; N, 12.80.

X-ray Crystallography. A pale blue regular prism was glued to the end of a glass fiber and mounted on either a Siemens SMART or Oxford Diffraction XCalibur X-ray diffractometer equipped with a CCD area detector. Full data sets were collected at 20, 150, and 298 K to monitor possible structural phase transitions of which none were identified. The area detector frames were integrated by use of the program SAINT[12] or CrysAlis CCD (Oxford Diffraction, Ltd.) and the resulting intensities corrected for absorption by Gaussian integration using the SHELXTL program suite[13] or CrysAlis RED (Oxford Diffraction, Ltd.). The SHELXTL program package was employed in the structure solution using direct methods, full matrix least-squares refinement on F^2 (using all data) and most graphics. All non-hydrogen atoms were refined anisotropically. Water hydrogen atoms were located by difference Fourier maps but ultimately fixed in calculated positions. Positions of aromatic H atoms were calculated by employing a "riding" model. No correction for extinction was required. Additional details of the data collection are given in Table 1 while selected bond lengths and angles are listed in Table 2.

Electron Spin Resonance. ESR spectra were recorded on an IBM ER-200 X-band spectrometer equipped with a TE_{102} microwave cavity. Single crystals were mounted at the end of a quartz rod, which could be rotated perpendicular to the field by use of a goniometer.

Magnetometry. DC magnetization measurements were conducted using a Quantum Design MPMS-7XL SQUID magnetometer. Homogeneous powder samples weighing 91.8 mg were loaded into gelatin capsules and mounted on the end of a carbon fiber rod. The samples were cooled in zero-field to the lowest achievable temperature of 2 K. The magnet was then charged to 1 kOe and data collected on warming up to 300 K. All magnetic data were corrected for core diamagnetism using Pascal's constants.

High-Field Magnetization. Magnetization (M) experiments were conducted to fields (B) of up to 65 T using the pulsed field magnets

---

(3) (a) Santoro, A.; Mighell, A. D.; Reimann, C. W. *Acta Crystallogr.* **1970**, *B26*, 979. (b) Hammar, P. R.; Stone, M. B.; Reich, D. H.; Broholm, C.; Gibson, P. J.; Turnbull, M. M.; Landee, C. P.; Oshikawa, M. *Phys. Rev. B* **1999**, *59*, 1008. (c) Losee, D. B.; Richardson, H. W.; Hatfield, W. E. *J. Chem. Phys.* **1973**, *59*, 3600.

(4) Lancaster, T.; Blundell, S. J.; Brooks, M. L.; Baker, P. J.; Pratt, F. L.; Manson, J. L.; Baines, C. *Phys. Rev. B* **2006**, *73*, 020410(R)

(5) Lancaster, T.; Blundell, S. J.; Brooks, M. L.; Baker, P. J.; Pratt, F. L.; Manson, J. L.; Baines, C. *Phys. Rev. B* **2006**, *73*, 172403.

(6) Manson, J. L.; Lancaster, T.; Chapon, L. C.; Blundell, S. J.; Schlueter, J. A.; Brooks, M. L.; Pratt, F. L.; Nygren, C. L.; Qualls, J. S. *Inorg. Chem.* **2005**, *44*, 989.

(7) (a) For example, see: (b) Woodward, F. M.; Albrecht, A. S.; Wynn, C. M.; Landee, C. P.; Turnbull, M. M. *Phys. Rev. B* **2002**, *65*, 144412. (c) Lindroos, S.; Lumme, P. *Acta Crystallogr.* **1990**, *C46*, 2039.

(8) (a) Lancaster, S. J.; Blundell, M. L.; Brooks, F. L; Pratt, J. L.; Manson, E. K; Brechin, C.; Cadiou, D; Low, E. J. L.; McInnes, R. E. P.; Winpenny, *J. Phys.: Condens. Mat.* **2004**, *16*, S4563. (b) Manson, J. L. Unpublished results.

(9) For example, (a) Swank, D. D.; Needham, G. F.; Willett, R. D. *Inorg. Chem.* **1979**, *18*, 761. (b) Willet, R. D.; Galeriu, C.; Landee, C. P.; Turnbull, M. M.; Twamley, B. *Inorg. Chem.* **2004**, *43*, 3804.

(10) Whangbo, M.-H.; Koo, H.-J.; Dai, D. *J. Solid State Chem.* **2003**, *176*, 417.

(11) (a) Abrahams, S. C. *J. Chem. Phys.* **1962**, *36*, 56. (b) Shulman, R. G.; Wyluda, B. J. *J. Chem. Phys.* **1961**, *35*, 1498. (c) Bozorth, R. M.; Nielsen, J. W. *Phys. Rev.* **1958**, *110*, 879.

(12) *SAINT*, Version 6.28a; Bruker AXS, Inc.: Madison, WI, 2001.

(13) Structure Solution and Refinement Software. *SHELXTL*, version 5.0; Bruker AXS, Inc.: Madison, WI, 1996.

Table 1. X-ray Crystallographic Refinement Details for $CuF_2(H_2O)_2(pyz)$

	T (K)		
	20	150	298
formula	$C_4H_8N_2O_2F_2Cu$	$C_4H_8N_2O_2F_2Cu$	$C_4H_8N_2O_2F_2Cu$
formula weight (g/mol)	217.66	217.66	217.66
crystal size, mm	0.45 × 0.35 × 0.30	0.56 × 0.44 × 0.28	0.38 × 0.36 × 0.32
space group	$P2_1/c$	$P2_1/c$	$P2_1/c$
a, Å	7.6250(10)	7.6617(12)	7.6926(6)
b, Å	7.5488(9)	7.5402(13)	7.5568(6)
c, Å	6.8453(9)	6.8674(11)	6.8970(5)
β, deg	112.029(13)	111.966(6)	111.065(3)
V, Å^3	365.25(9)	367.93(10)	374.14(5)
Z	2	2	2
ρ_{calcd}, g/cm^3	1.979	1.965	1.932
λ, Å	0.71073	0.71073	0.71073
μ, mm^{-1}	2.978	2.956	2.907
$R(F)^a$	0.0257	0.0234	0.0159
$R_w(F^2)^b$	0.0720	0.0831	0.0511
GOF	1.191	1.219	1.109

[a] $R = \Sigma||F_o| - |F_c||/\Sigma|F_o|$. [b] $R_w = [\Sigma w[|F_o| - |F_c|]^2/\Sigma w[|F_o|^2]]^{1/2}$.

Table 2. Selected Bond Lengths (Å) and Bond Angles (deg) for $CuF_2(H_2O)_2(pyz)$

T (K)	20	150	298
Cu−O	1.978(2)	1.979(2)	1.981(1)
Cu−F	1.916(2)	1.911(1)	1.904(1)
Cu−N	2.422(2)	2.438(2)	2.455(1)
O−Cu−F	89.25(4)	89.27(4)	89.35(3)
O−Cu−N	88.53(7)	88.66(7)	88.53(5)
N−Cu−F	87.72(5)	87.86(4)	88.36(3)
H(3)−O−H(4)	107(4)	107(4)	106(3)

of the National High Magnetic Field Laboratory in Los Alamos, NM. An extraction magnetometer[14] was used to measure aligned single crystals of $CuF_2(H_2O)_2(pyz)$; the magnetometer was placed inside a standard ^{3}He cryostat providing temperatures down to 0.4 K.

Muon-Spin Relaxation. Zero-field muon-spin relaxation (ZF-μSR) measurements were conducted on a powder sample of $CuF_2(H_2O)_2(pyz)$ using the MuSR instrument at the ISIS facility, Rutherford Appleton Laboratory, U.K. In a typical μSR experiment[15] spin-polarized positive muons are stopped in a target sample, where the muon usually occupies an interstitial position in the crystal. The observed property in the experiment is the time evolution of the muon spin polarization, the behavior of which depends on the local magnetic field at the muon site. Each muon decays, with a lifetime of 2.2 μs, into two neutrinos and a positron, the latter particle being emitted preferentially along the instantaneous direction of the muon spin. Recording the time dependence of the positron emission directions therefore allows the determination of the spin-polarization of the ensemble of muons. In our experiments positrons are detected by detectors placed forward (F) and backward (B) of the initial muon polarization direction. Histograms $N_F(t)$ and $N_B(t)$ record the number of positrons detected in the two detectors as a function of time following the muon implantation. The quantity of interest is the decay positron asymmetry function, defined as

$$A(t) = \frac{N_F(t) - \alpha_{exp}N_B(t)}{N_F(t) + \alpha_{exp}N_B(t)} \qquad (1)$$

where α_{exp} is an experimental calibration constant. $A(t)$ is proportional to the spin polarization of the muon ensemble. For these measurements, a standard orange cryostat and a sorption cryostat were used,[15] with a powder sample packed in a silver foil packet (foil thickness 25 μm) and mounted on a silver backing plate.

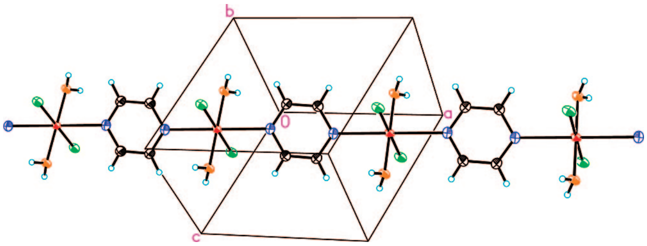

Figure 1. ORTEP diagram and atom labeling scheme for a segment of a 1D linear chain of $CuF_2(H_2O)_2(pyz)$. Thermal ellipsoids are drawn at the 35% probability level. Red, blue, yellow, black, green, and cyan ellipsoids represent Cu, N, O, C, F, and H atoms, respectively.

Theoretical Calculations. To evaluate the spin exchange parameters for various spin exchange paths of $CuF_2(H_2O)_2(pyz)$, first principles density functional theory (DFT) spin-polarized electronic structure calculations were carried out for the high-spin (HS) and broken-symmetry (BS) states of the spin dimers associated with the spin exchange paths (i.e., structural units consisting of two adjacent Cu^{2+} ion sites, see Section 4). Our calculations were carried out by employing the B3LYP exchange-correlation functional [16,17] and the basis sets 6-31G* and 6-311G** encoded in the Gaussian 03, revision B.04, program package.[18] The electronic energies of the HS and BS states of a spin dimer are defined as E_{HS} and E_{BS}, respectively. Since each spin site of $CuF_2(H_2O)_2(pyz)$ has the spin-1/2 Cu^{2+} ion, the exchange parameter J associated with a spin dimer is related to E_{HS} and E_{BS} as follows:[19,20]

$$J = (E_{BS} - E_{HS}) \qquad (2)$$

3. Crystal Structure

Uniform 1D linear chains (Figure 1) are assembled from pyrazine bridges that link the $CuF_2O_2N_2$ octahedra together along the a-axis leading to intrachain Cu···Cu separations of 7.625(1) Å at room temperature. By comparison, the intrachain Cu···Cu distance in $Cu(NO_3)_2(pyz)$ is ~1 Å shorter at 6.71 Å.[3] In the fluoride compound, the pyz bridge makes an angle of 50.34(7)° relative to the ab-plane. The molecular geometry of pyz is in good agreement with those reported earlier.[2,3]

Extensive hydrogen bonding interactions link the chains into a rigid 3D network as shown in Figure 2a, where each F^- forms an H-bond with two water molecules from two different chains. These interchain interactions consist of two slightly different F···H−O linkages where the F···O distances are 2.612 and 2.597 Å while their associated F···H(3)−O and F···H(4)−O bond angles are 166.8 and 170.9°, respectively, at room temperature. The F···O bond distances are comparable to 2.507 Å and 2.592 Å found in $[L^5Cu_2F(H_2O)_2(CH_3OH)](BF_4)_2$ (L^5 is a chelating pyrazolate-

---

(14) Goddard, P. A.; Singleton, J.; Sengupta, P.; McDonald, R. D.; Lancaster, T.; Blundell, S. J.; Pratt, F. L.; Cox, S.; Harrison, N.; Manson, J. L.; Southerland, H. I.; Schlueter, J. A. *New J. Phys.* **2008**, *10*, 083025.

(15) (a) Blundell, S. J. *Contemp. Phys.* **1999**, *40*, 175. (b) http://www.isis.rl.ac.uk/muons/musr/ index.html.

(16) Becke, D. *Phys. Rev. A* **1988**, *38*, 3098.

(17) Lee, C.; Yang, W.; Parr, R. G. *Phys. Rev. B* **1988**, *37*, 785.

(18) Frisch, M. J.; et al. *Gaussian 03*, Revision B.04, Gaussian, Inc.: Pittsburgh, PA, 2003.

(19) Noodleman, L. *J. Chem. Phys.* **1981**, *74*, 5737.

(20) Dai, D.; Whangbo, M.-H. *J. Chem. Phys.* **2001**, *114*, 2887.

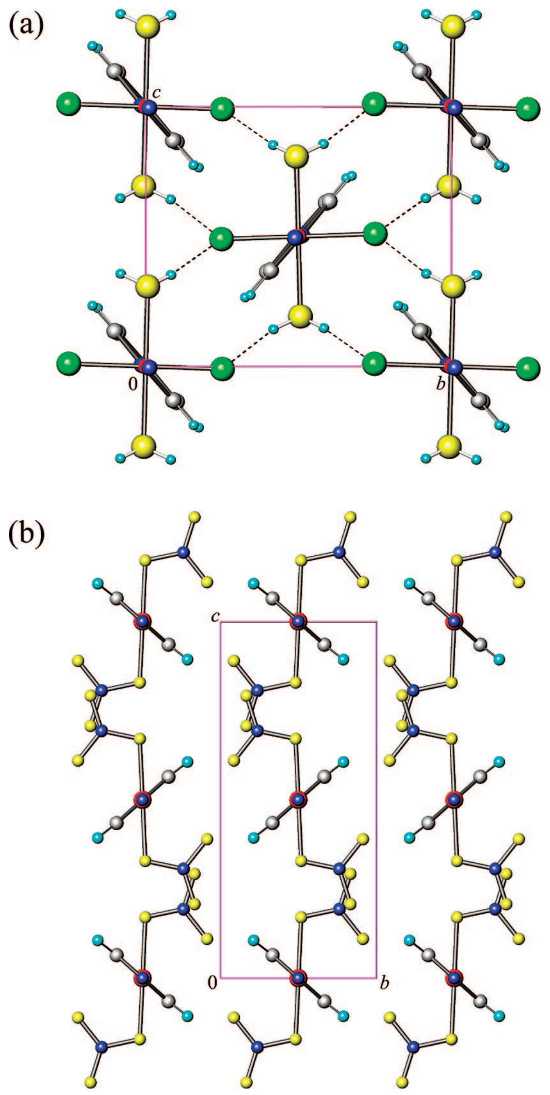

Figure 2. Chain packing arrangements for (a) $CuF_2(H_2O)_2(pyz)$ and (b) $Cu(NO_3)_2(pyz)$ viewed along the chain axis. Dashed lines in (a) delineate F···H−O hydrogen bonds. Red, blue, yellow, gray, green, and cyan spheres represent Cu, N, O, C, F, and H atoms, respectively.

based ligand) and $CuF_2(H_2O)_2$, respectively.[21,22] An interesting aspect of $CuF_2(H_2O)_2(pyz)$ is that, according to recent temperature-dependent IR spectroscopic measurements,[23] the H−O−H bond angle increases upon cooling hence strengthening the F···H−O hydrogen bond.

When viewed parallel to the *a*-axis, it can be seen that neighboring chains counter-rotate by ± 2.62(1)° along the *bc*-diagonals due to the strong electrostatic interaction between the highly electro-positive and negative H/F-atoms; this packing scheme contrasts that of $Cu(NO_3)_2(pyz)$ as depicted in Figure 2b. Considering only the H-bonded network in the fluoride compound, a planar quasi-2D net results giving intermolecular Cu···Cu separations of 7.5488(9) and 6.8453(9) Å along the *b*- and *c*-directions, respectively. Hence, the hydrogen bond network can be described as a quasi-2D lattice.

The crystal structures of $CuF_2(H_2O)_2(pyz)$ determined at temperatures of 20, 150, and 298 K show little variation in the unit cell parameters but were necessary to rule out structural phase changes. These variations are highlighted in Tables 1 and 2. Between 20 and 298 K, the *a*, *b*, and *c* lattice parameters vary by less than 1% while the β-angle decreases by ∼1° upon warming over that temperature range. Collectively, these changes result in the gradual expansion of the unit cell volume by 2.4% as the temperature increases. We note that no structural phase transitions were observed, which is consistent with a recent IR spectroscopic investigation.[23]

Each $CuF_2N_2O_2$ octahedron exhibits an axial elongation expected for a Jahn−Teller active Cu^{2+} ion, with the Cu−N bonds as the axial ligands and the Cu−F and Cu−O bonds forming a square plane. The geometry of each $CuF_2N_2O_2$ octahedron is little affected by temperature as gleaned from Table 2. While the Cu−O bond length remains unchanged (within experimental error), the Cu−F and Cu−N bonds slightly increase and decrease, respectively, as the material is cooled. Clearly, the axial elongation associated with the Jahn−Teller distortion remains along the N−Cu−N direction at all temperatures. The bond angles within the Cu chromophore are largely invariant as the temperature is changed. In addition, the H(3)−O−H(4) bond angle is nearly unaltered, but it should be mentioned that IR studies made on a single crystal indicate a widening of this angle upon cooling along with a concomitant strengthening of the F···H−O hydrogen bond network.[23] Neutron diffraction experiments are in progress to better resolve the hydrogen bonding geometry.

4. Magnetic Orbital Plane and Spin Exchange Interactions

As discussed in the previous section, the axially elongated local geometry of the $CuF_2O_2N_2$ octahedron indicates that the magnetic orbital $d_{x^2-y^2}$ of the Cu^{2+} ion lies in the CuF_2O_2 plane. To confirm this point, first principles DFT spin-polarized calculations were performed for the spin monomer $CuF_2(OH_2)_2(pyz)_2$ of $CuF_2(H_2O)_2(pyz)$. The magnetic orbital $d_{x^2-y^2}$ of the Cu^{2+} ion is calculated to be in the CuF_2O_2 plane by the basis sets 6-31G* and 6-311G**, hence indicating that the nearest-neighbor spin exchange interaction J_{2D} within the *bc*-plane would be substantial leading to a 2D spin lattice (Figure 3). If the magnetic orbital were contained in the CuF_2N_2 plane, the nearest-neighbor spin exchange interaction $J_\perp$ along the *a*-direction would be substantial leading to a 1D spin lattice. The spin dimer representing J_{2D} is $[Cu(OH_2)_2F_2(pyz)_2]_2$ (Figure 4a) and that representing $J_\perp$ is $[(pyz)F_2(H_2O)_2Cu\text{-}pyz\text{-}Cu(OH_2)_2F_2(pyz)]$ (Figure 4b). The values of J_{2D} and $J_\perp$ determined by calculating the HS and BS states of these spin dimers are summarized in Table 3, which shows that the spin exchange J_{2D} is antiferromagnetic and is much stronger than the spin exchange $J_\perp$ as expected from the fact that the magnetic orbital lies in the CuF_2O_2 plane.

For a Cu^{2+} ion located in an axially elongated octahedral site, the *g*-factor parallel $g_{||}$ to the axial direction (i.e., the

---

(21) Ackermann, J.; Meyer, F.; Pritzkow, H. *Inorg. Chim. Acta* **2004**, *357*, 3703.

(22) (a) Abrahams, S. C.; Prince, E. *J. Chem. Phys.* **1962**, *36*, 50. (b) Prince, E. *J. Chem. Phys.* **1972**, *56*, 4352.

(23) Brown, S.; Cao, J.; Musfeldt, J.; Conner, M. M.; McConnell, A. C.; Southerland, H. I.; Manson, J. L.; Schlueter, J. A.; Phillips, M. D.; Turnbull, M. M.; Landee, C. P. *Inorg. Chem.* **2007**, *46*, 8577.

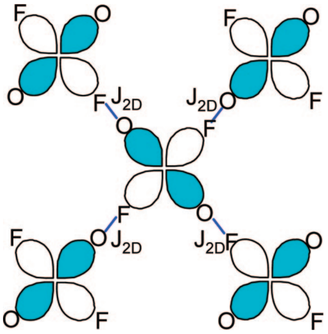

Figure 3. Illustration showing the primary supersuperexchange paths, J_{2D}, between hydrogen bonded $CuF_2O_2N_2$ octahedra. The short blue line represents the F•••H−O hydrogen bond interaction.

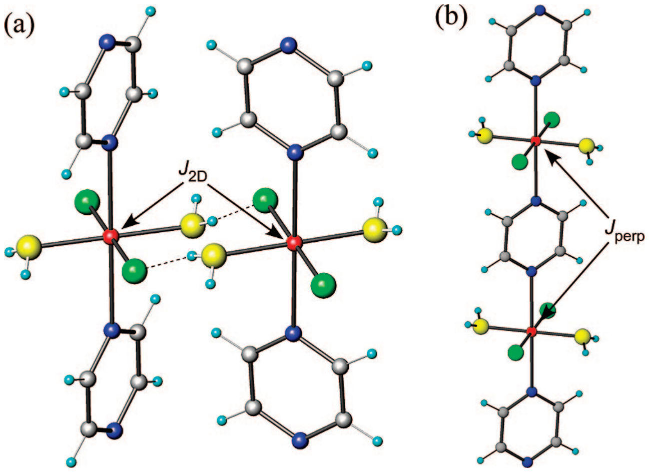

Figure 4. Spin dimers representing the spin exchange interactions between two Cu sites: (a) J_{2D} and (b) J_{perp} as used in the DFT study. The Cu, F, O, N, C, and H atoms are represented by red, green, yellow, blue, gray, and cyan spheres, respectively.

Table 3. Values of the Spin Exchange Parameters J_{2D} and $J_\perp$ Estimated from First Principles DFT Calculations

	J_{2D}/k_B (K)	$J_\perp/k_B$ (K)
6-31G*	−13	−0.13
6-311G**	−19	−0.13

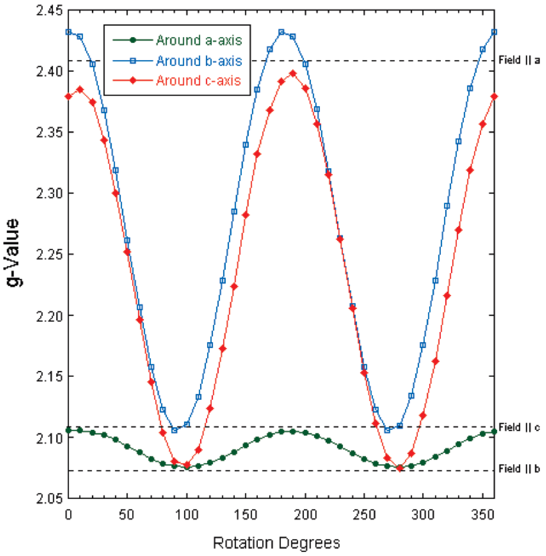

Figure 5. Angular-dependence of the g-tensor for a single crystal of $CuF_2(H_2O)_2(pyz)$ determined from the room temperature ESR data.

local z-axis direction perpendicular to the plane of the magnetic orbital) is greater than the g-factor $g_\perp$ perpendicular to the axial direction (i.e., the direction parallel to the plane of the magnetic orbital). For example, $g_\parallel = 2.22$ and $g_\perp = 2.05$ for the Cu^{2+} ion of $Cu(NH_3)_4SO_4 \cdot H_2O$.[24] The observed g-factors differ from the value of 2 because of spin−orbit coupling.[25] The deviation $\Delta g_\parallel = g_\parallel - 2$ arises largely from the mixing of the d_{xy} state into the $d_{x^2-y^2}$ state induced by spin−orbit coupling, and the deviation $\Delta g_\perp = g_\perp - 2$ largely from the mixing of the d_{xz} and/or d_{yz} state into the $d_{x^2-y^2}$ state. $\Delta g_\parallel$ is greater than $\Delta g_\perp$, because the mixing of the d_{xy} state into the $d_{x^2-y^2}$ state is more efficient than that of the d_{xz} and/or d_{yz} state into the $d_{x^2-y^2}$ state.

The CuF_2O_2 plane of $CuF_2(H_2O)_2(pyz)$ is almost perpendicular to the a-axis and is tilted out of the bc-plane by 23.5°. Thus, the g-factor of the Cu^{2+} ion would be close to $g_\parallel$ along the a-direction and to $g_\perp$ along the direction perpendicular to the a-axis. Consequently, one can verify whether or not the magnetic orbital of the Cu^{2+} ion lies in the CuF_2O_2 plane by measuring with ESR how the g-factors of a single crystal sample of $CuF_2(H_2O)_2(pyz)$ vary as it is rotated around the crystallographic axes within the ESR cavity (see Figure 5). For $S = 1/2$ systems, the angular dependence of the g-factor is determined by the projection of the field leading to the sinusoidal dependence observed in Figure 5

$$g(\theta) = \sqrt{{g_\perp}^2 \sin^2 \theta + {g_\parallel}^2 \cos^2 \theta} \tag{3}$$

where θ is the angle between the z-axis and the plane of the magnetic orbital. For the rotation around the b- or c-axes the g-factor variation is strong. This means that the magnetic orbital plane can be parallel or perpendicular to the magnetic field during rotation around these axes. This is possible only if the magnetic orbital lies in the CuF_2O_2 plane. For the rotation around the a-axis, the g-factor is small, but its angular dependence is nonzero. This reflects the fact that the Cu site symmetry in $CuF_2(H_2O)_2(pyz)$ is slightly lower than tetragonal, and hence the d_{xz} and d_{yz} states are not degenerate. Thus, the observed angular dependence of the g-factor for $CuF_2(H_2O)_2(pyz)$ (Figure 5) shows clearly that the plane of the magnetic orbital is in the CuF_2O_2 plane.

5. Magnetic Susceptibility and Magnetization

The magnetic properties of $CuF_2(H_2O)_2(pyz)$ were measured between 2 and 300 K. Figure 6 shows χ vs T with χT vs T plot in the inset. χ reaches a broad maximum at 10.5 K, due to the development of short-range correlations characterized by an energy scale given by J_1, the dominant exchange coupling in the system. Below 10.5 K, the susceptibility decreases smoothly and then rises abruptly near 4.3 K. The rapid increase in χ continues to the lowest measured temperature of 2 K, reaching a value of 0.038 emu/mol. It should be noted that this feature is not due to a paramagnetic impurity because ac susceptibility (see Supporting Information) studies to slightly lower temperatures show a sharp peak in χ' at ~2.5 K although no anomaly

---

(24) Carson, E. H.; Spence, R. D. *J. Chem. Phys.* **1956**, *24*, 471.
(25) Pryce, M. H. L. *Proc. Phys. Soc. London, Ser. A* **1950**, *63*, 25.

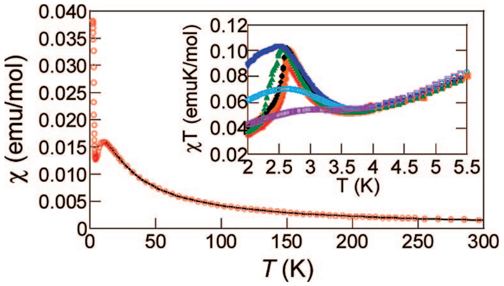

Figure 6. χ vs T (main) and χT vs T (inset) plots for polycrystalline $CuF_2(H_2O)_2(pyz)$. The solid line in the main plot represents a theoretical fit to the $S = 1/2$ 2D quadratic antiferromagnet as described in the text. For the inset, the data were obtained in external fields of 50 G (red), 100 G (orange), 250 G (black), 500 G (green), 1000 G (blue), 2500 G (cyan), and 5000 G (purple).

was found in χ'', which is consistent with the possibility of a weak spin-canting (see below for further discussion).

The broad χ_{max} seen in Figure 6 occurs at a temperature higher than that found for 1D $Cu(NO_3)_2(pyz)$ ($T_{max} = 6.8$ K).[3b,c] A Curie−Weiss fit of χ between 35 and 300 K gave $g = 2.28(1)$ and $\theta = -15.1(1)$ K, which indicates the presence of dominant antiferromagnetic coupling between the spin-1/2 Cu^{2+} ions. The g-value obtained from the fit reflects the usual anisotropy of the Cu^{2+} g-tensor as confirmed by ESR measurements. At 300 K, the value of χT is 0.465 emuK/mol, which is larger than the value expected for isolated spin-1/2 ions (i.e., 0.375 emu K/mol). Upon cooling, χT decreases continuously until ~50 K, below which it falls off much more rapidly owing to enhanced antiferromagnetic correlations between Cu^{2+} sites. The inset of Figure 6 shows that χT is strongly field-dependent below 3.5 K. The field-dependence of χT is most likely due to a weak ferromagnetic interaction or the onset of a spontaneous magnetic moment as a result of spin canting.[1a] A similar behavior has been recently reported in $Cu(trz)(N_3)$ (trz = 1,2,4-triazole).[26] Spin canting can occur in systems that lack inversion symmetry and/or possess antisymmetric exchange induced by the Dzyaloshinskii-Moriya (DM) interaction.[27] The inset of Figure 6 shows that at a field lower than 500 G, χT initially increases below 3.5 K reaching a maximum around 2.6 K and rapidly decreases below 2.6 K. This general behavior can be understood by supposing a spin canting in each 2D layer, which will increase χT below 3.5 K. The sharp decrease in χT below the peak can be explained by supposing an interlayer antiferromagnetic order. At magnetic fields above 1000 G, the χT vs T peak below 2.6 K is replaced with a χT vs T plateau, which suggests a decoupling of the interlayer interactions. Furthermore, the gradual lowering of the χT vs T plateau below 2.6 K with increasing the magnetic field suggests the decrease in the extent of spin canting in each 2D layer. Antisymmetric magnetic exchange must be responsible for the observed spin canting because $CuF_2(H_2O)_2(pyz)$ does in fact have an inversion center. In order to further evaluate the origin of the spin canting in $CuF_2(H_2O)_2(pyz)$, we plan to investigate the spin configuration of the magnetic ground-state by neutron scattering, magnetic susceptibility, and magnetization measurements on single crystals.

The Jahn−Teller distortion around each $CuF_2N_2O_2$ octahedron suggests that its magnetic orbital is contained in the CuF_2O_2 plane, as verified by the present first principles DFT calculations and ESR measurements. Our evaluation of the spin exchange interactions showed that the spin lattice model most appropriate for describing the magnetic properties of $CuF_2(H_2O)_2(pyz)$ is a 2D square net made up of the nearest-neighbor spin exchange interactions J_1 through the Cu−F··· HO−Cu paths. Thus, the $\chi(T)$ data were least-squares fitted to a $S = 1/2$ 2D Heisenberg square lattice model based on the Hamiltonian $H = -J_{ij}\sum S_i \cdot S_j$.[7a] In order to account for possible exchange along the Cu−pyz−Cu direction, our model included a mean-field correction term.[28] An excellent agreement was obtained between 10 and 300 K for the parameters $g = 2.24(1)$, $J_{2D}/k_B = -5.58(1)$ K, $zJ_\perp/k_B = -0.4(1)$ K, and $R = 1.9 \times 10^{-9}$ (where $R = \sum[\chi_{obsd} - \chi_{calcd}]^2/\sum[\chi_{obsd}]^2$). As an independent assessment of the J_{2D}/k_B value, we can use the relationship between J_{2D} and T_{max} (i.e., the temperature at which the magnetic susceptibility reaches a maximum) for a 2D Heisenberg square lattice model, $|k_B T_{max}/J_{2D} S(S + 1)| = 2.53$. This relationship gives rise to $|J_{2D}/k_B| = 5.5$ K, in good agreement with the value determined from the 2D fit.[29] The calculated J_{2D}/k_B value (see Table 3) is greater than the experimental value by a factor of 2−3, which is reasonable since DFT calculations tend to overestimate spin exchange parameters by a factor of approximately up to four.[30] The calculated $J_\perp/k_B$ value is small in magnitude, which is consistent with the fact that the $zJ_\perp/k_B$ value is small in magnitude. The g-value is consistent with that obtained from the Curie−Weiss fit and the experimental ESR data. A similar exchange network may be operative in $CuF_2(H_2O)_2$, but this point has not been raised previously and the primary exchange path has been thought to be along the Cu−F−Cu chain direction.[10] We can compare the general chain structure of $CuF_2(H_2O)_2(pyz)$ to the isolated chains of $Cu(hfac)_2(pyz)$ (hfac = hexafluoroacetylacetonate)[31] which also experiences a long Cu−N bond (2.53 Å). In the hfac-derivative, it was found that there was negligible exchange coupling ($\theta = -0.54$ K) along the chain direction because the $d_{x^2-y^2}$ magnetic orbital is oriented in the CuO_4 plane, the same scenario encountered in $CuF_2(H_2O)_2(pyz)$, which due to extensive strong interchain hydrogen bonding, produces a spin-ordered magnet.

Figure 7a shows typical high-field $M(B)$ data for temperatures of 0.5, 1.5, 4.1, and 10 K. At the higher temperatures, $M(B)$ is convex, showing a gradual approach to saturation at high fields. However, as the temperature is lowered, the $M(B)$ data become concave at lower fields, with a rounded, "elbow"-like transition to a constant saturation magnetization M_{sat}. We label the field at which the "elbow" occurs as B_c.

---

(26) Li, J.-R.; Yu, Q.; Sanudo, E. C.; Tao, Y.; Bu, X.-H. *Chem. Commun.* **2007**, 2602.

(27) Dzyaloshinsky, I. *J. Phys. Chem. Solids* **1958**, *4*, 241.

(28) Ginsberg, A. P.; Lines, M. E. *Inorg. Chem.* **1972**, *11*, 2289.

(29) de Jongh, L. J.; Miedema, A. R. *Adv. Phys.* **1974**, *23*, 1.

(30) (a) Dai, D.; Whangbo, M.-H. *J. Chem. Phys.* **2001**, *114*, 2887. (b) Dai, D.; Whangbo, M.-H.; Koo, H.-J.; Rocquefelte, X.; Jobic, S.; Villesuzanne, A. *Inorg. Chem.* **2005**, *44*, 2407. (c) Grau-Crespo, R.; de Leeuw, N. H.; Catlow, C. R. *J. Mater. Chem.* **2003**, *13*, 2848.

(31) (a) Belford, R. C. E.; Fenton, D. E.; Truter, M. R. *J. Chem. Soc., Dalton Trans.* **1974**, 17. (b) Richardson, H. W.; Wasson, J. R.; Hatfield, W. E. *Inorg. Chem.* **1977**, *16*, 484.

As shown in Figure 7a, B_c depends on the crystal's orientation in the applied field and was found to occur at 28.8 and 33.1 T when B is aligned parallel or perpendicular to the *a*-axis, respectively. However, the magnetization data for both orientations become identical to within experimental uncertainty when plotted as M/M_{sat} versus gB (Figure 7b); here, g is the Landé g-factor, as measured by ESR, appropriate for that direction of magnetic field. This strongly suggests that the g-factor anisotropy is entirely responsible for the observed angle dependence of the critical field and that the relevant energy scale for the magnetization is gB.[14]

In another paper,[14] we carried out Quantum Monte-Carlo simulations of a 2D Heisenberg square lattice with an additional interlayer exchange coupling energy, $J_\perp$, that quantitatively reproduce data such as those in Figure 7; the degree of concavity depends on the effective dimensionality of the system, while the field B_c at which the "elbow" occurs is an accurate measure of the in-plane exchange energy, where $|J_{2D}| = gB_c/6.03$.

Using the data in Figure 7b and the known g-factors, we can therefore obtain another measurement of the in-plane exchange energy, $|J_{2D}| = 5.8(2)$ K. This value may be combined with the Neel temperature of 2.54 K obtained from μSR to yield an anisotropy of $|J_{2D}/J_\perp| \approx 4 \times 10^{-4}$ using the procedure described in ref 14.

In Figure 7c we highlight the low-field region of $M(B)$ measured using a SQUID magnetometer. Above and below the sharp step at ~500 G, the magnetization rises nearly linearly which is consistent with prominent antiferromagnetic correlations. The discontinuity is likely due to a spin-flop phase transition, B_{sf}, and because it occurs at such a low field suggests the presence of a weak spin anisotropy.[29] The spin flop-to-paramagnetic phase transition occurs at B_c as discussed above. Knowing both B_{sf} and B_c we can employ mean-field expressions (eqs 4 and 5) derived for $T = 0$ to extrapolate the exchange (B_E) and anisotropy fields (B_A);[29] we calculate upper limits of B_E and B_A to be 16.55 and 0.0015 T, respectively.

$$B_{SF} = \sqrt{2B_E B_A - {B_A}^2} \tag{4}$$

$$B_c = 2B_E - B_A \tag{5}$$

In order to estimate the spin canting angle, the magnitude of the remnant magnetization, B_{rem}, must be known. Unfortunately the presence of the spin flop transition masks any hysteretic behavior needed to determine B_{rem} although it is likely that the canting angle is less than 1° due to the weak anisotropy. We stress the need for additional data made on oriented single crystals in order to comment further.

6. Muon Spin Relaxation

6.1. Magnetically Ordered State. Example ZF-μ^+SR spectra measured on $CuF_2(H_2O)_2(pyz)$ are shown in Figure 8a,c. Below a temperature $T = 2.62$ K oscillations in the asymmetry spectra are observed at several frequencies (Figure 8a). These oscillations are characteristic of a quasi-static local magnetic field at the muon stopping site, which causes a coherent precession of the spins of those muons with a component of their spin polarization perpendicular to this local field (expected to be 2/3 of the total polarization). The frequency of the oscillations is given by $\nu_i = \gamma_\mu B_i/2\pi$, where γ_μ is the muon gyromagnetic ratio ($= 2\pi \times 135.5$ MHz/T) and B_i is the magnitude of the local magnetic field at the ith muon site. Any distribution in magnitude of these local fields will result in a relaxation of the oscillating signal, described by relaxation rates λ_i. The presence of oscillations at low temperatures in $CuF_2(H_2O)_2(pyz)$ suggests very strongly that this material is magnetically ordered below 2.62 K. Three separate frequencies were identified in the low temperature spectra, corresponding to three magnetically inequivalent muon sites in the material. The precession frequencies, which are proportional to the internal magnetic field as experienced by the muon, may be viewed as an effective order parameter for the system. In order to extract the T-dependence of the frequencies, the low temperature data were fitted to the functional form,

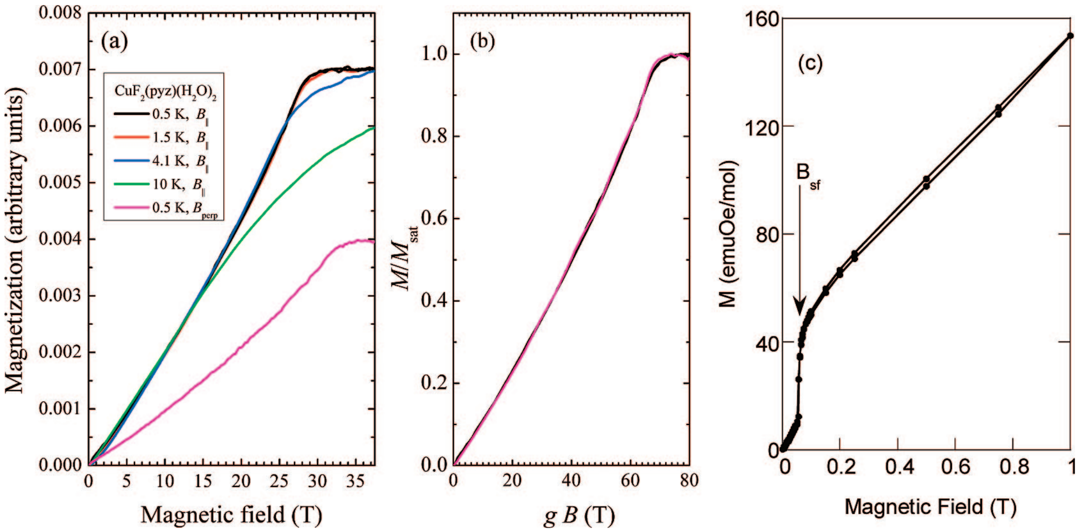

Figure 7. (a) $M(B)$ of a $CuF_2(H_2O)_2(pyz)$ single crystal with B applied parallel to ($B_\parallel$; $T = 0.5$, 1.5, 4.1, and 10 K) and perpendicular to ($B_\perp$; $T = 0.5$ K) the crystallographic *a*-axis. (b) The 0.5 K data from (a) plotted as M/M_{sat} versus gB, where g is the appropriate g-factor for the particular B direction ($g = 2.42$ for $B_\parallel$ and 2.09 for $B_\perp$).[14] Note that both data sets collapse onto a single curve, showing that the relevant energy scale determining M is gB. (c) Low-field $M(B)$ at 2 K for a polycrystalline sample showing the spin-flop transition, B_{sf}.

$$A(t) = A_1 \exp(-\lambda_1 t)\cos(2\pi\nu_1 t + \phi_1) + A_2 \exp(-\lambda_2 t) \times \cos(2\pi\nu_2 t + \phi_2) + A_3 \exp(-\lambda_3 t)\cos(2\pi\nu_3 t + \phi_3) + A_4 \exp(-\lambda_4 t) + A_{bg} \exp(-\lambda_{bg} t) \quad (6)$$

where the term $A_4 \exp(-\lambda t)$ accounts for the contribution from those muons with a spin component parallel to the local magnetic field and $A_{bg} \exp(-\lambda_{bg} t)$ reflects the small signal from those muons that stop in the silver sample holder or cryostat tail. We note that phase offsets ϕ were required to fit the data (see Table 4) as observed in our previous μ^+SR studies of Cu^{2+} systems.[4-6,8] The amplitudes of the oscillating components were found to be roughly A_1:A_2:A_3 = 4:2:1, suggesting that the three muon sites have occupation probabilities 4/7:2/7:1/7. The three frequencies were found to be in the proportions ν_1:ν_2:ν_3 = 1:0.65:0.55 and were fixed in this ratio during the fitting procedure. The resulting temperature evolution of the precession frequencies is shown in Figure 8b. For $1.47 \le T \le 2.62$ K, the other parameters in eq 4 were fixed at the values given in Table 4. The pulsed structure of the beam at the ISIS facility limits the dynamic range of measurements to below ~5 MHz. This causes difficulties in fitting the higher frequency oscillations observed at low temperatures. For $T < 1.47$ K, the relaxation rates λ_i were therefore allowed to vary. These considerations account for the scatter in the data seen for $T < 1.45$ K (Figure 8b). Measurements made close to the critical temperature allow an effective order parameter to be extracted in the critical region (Figure 8c). Fitting these data to the functional form, $(T_N - T)^\beta$ yields T_N = 2.59(1) K and β = 0.36(1).

Table 4. Fitting Parameters for Equation 2 Applied to Data Measured in the Magnetically Ordered State

i	A_i (%)	λ_i (MHz)	ϕ_i (deg)
1	1.77	2.28	−38.0
2	0.877	1.90	−0.8
3	0.44	0.89	161.8
4	3.02	0.19	

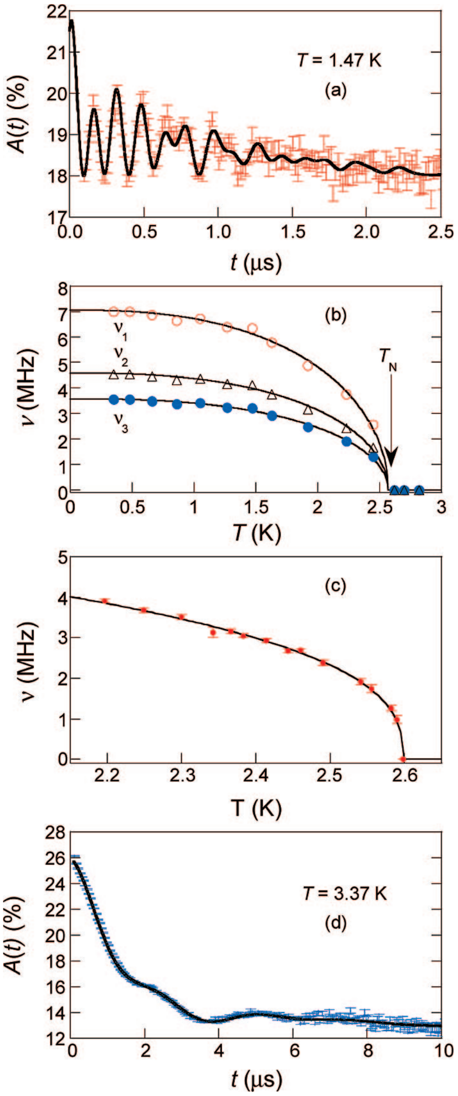

Figure 8. (a) ZF μ+SR spectrum measured at 1.47 K showing oscillations at three distinct frequencies. The solid line is a fit to eq 4. (b) Temperature-evolution of the three muon precession frequencies. The solid lines serve as guides to the eye. (c) T-dependence of the critical region from which T_N and β were extracted. (d) ZF spectrum measured at 3.37 K showing low frequency oscillations attributable to nuclear dipole effects. A fit is shown to a muon−fluorine dipole−dipole interaction model as described in ref 29.

6.2. Paramagnetic State. An example spectrum showing the observed asymmetry above T_N is shown in Figure 8d. Low amplitude oscillations are seen at a number of frequencies persisting to above 100 K, with little change over the measured temperature range. This temperature dependence implies that these oscillations are not attributable to static magnetic order but rather to the quantum entanglement of the muon spin and the nuclear moment of a fluorine nucleus near the muon stopping site.[32] In $CuF_2(H_2O)_2(pyz)$ the observed spectra correspond to the muon interacting with a single fluorine nucleus. The interaction is highly sensitive to muon−fluorine separation and allows us to identify a muon site separated from a fluorine nucleus by 0.11 nm (see ref 32 for a discussion).

7. Concluding Remarks

The 3D coordinate polymer $CuF_2(H_2O)_2(pyz)$ is made up of distorted $CuF_2(H_2O)_2(pyz)_2$ octahedra which are tethered together by strong F•••H−O hydrogen bonds forming a 2D square lattice that is linked in the third direction by pyz linkages. The g-factor measurements by ESR and first principles DFT calculations show that the magnetic orbital of each Cu^{2+} ion lies in the CuF_2O_2 plane and the magnetic properties of $CuF_2(H_2O)_2(pyz)$ should be described by a 2D antiferromagnetic square lattice. The magnetic susceptibility of $CuF_2(H_2O)_2(pyz)$ is well fitted by this model with J_{2D}/k_B = −5.58(1) K. At ~2.6 K $CuF_2(H_2O)_2(pyz)$ undergoes a transition to a long-range magnetic ordering, which is attributed to a spin-canted state that is induced by the strengthening of the F•••H−O hydrogen bond network when the temperature is lowered. Our work shows that the 3D magnetic ordering temperature and the type of magnetic ordering can be affected by hydrogen bonding. While 1D chains are formed in $CuF_2(H_2O)_2(pyz)$ and $Cu(NO_3)_2(pyz)$, the presence of strong hydrogen bonds in the former causes the chains to alter their packing arrangement, thus leading to a novel ground-state characterized by spin-canting and a dramatically increased critical temperature, which is ~25

---

(32) Lancaster, T.; Blundell, S. J.; Baker, P. J.; Hayes, W.; Pratt, F. L.; Manson, J. L.; Conner, M. M.; Schlueter, J. A. *Phys. Rev. Lett.* **2007**, *99*, 267601.

times higher than that observed in $Cu(NO_3)_2$(pyz). Our study clearly demonstrates that strong hydrogen bonds such as those exhibited by F•••H−O (and possibly F•••H−N) should be studied further to evaluate their ability to mediate supersuperexchange interactions. Future studies on $CuF_2(H_2O)_2$(pyz) will involve heat capacity and neutron scattering on single crystals to determine the *H*/*T* phase diagram of this system in order to better understand the nature of the supersuperexchange mechanism. Together with pyrazine-derivatives, we are continuing to explore Cu^{2+} and other divalent transition metal ions to further develop related materials.

Acknowledgment. This research was supported by an award from Research Corporation (J.L.M.). Work supported by UChicago Argonne, LLC, operator of Argonne National Laboratory (“Argonne”). Argonne, a U.S. Department of Energy Office of Science Laboratory, is operated under contract No. De-AC02-06CH11357. Research performed at North Carolina State University was supported by the Office of Basic Energy Sciences, Division of Materials Sciences of the U.S. Department of Energy under Grant DE-FG02-86ER45259, respectively. We are grateful to P. King (ISIS) and L. Vendier (LCC) for technical assistance. This work was also supported by the EPSRC. T.L. acknowledges support from the Royal Commission for the exhibition of 1851 (U.K.).

Supporting Information Available: $\chi'(T)$ plot for a polycrystalline sample of $CuF_2(H_2O)_2$(pyz) (PDF) and crystallographic information (CIF). This material is available free of charge via the Internet at http://pubs.acs.org.

CM8016566